## Broader context

Efficient production of hydrogen from water through electrocatalysis represents a promising route to a clean and renewable energy carrier. To this end, numerous important reports have been made on the design of effective earth-abundant materials. Nevertheless, in comparison with Pt, much work remains necessary to decrease the overpotentials required to drive efficiently the hydrogen evolution reaction (HER) with inexpensive electrocatalysts. Our strategy to achieve this goal was to provide experimental evidence of the predicted beneficial "microenvironment effect", for the HER, which should result from the combination, in a 3D configuration, of high-quality reduced graphene oxide (rGO) nanosheets and a polyoxometalate $[H_7P_8W_{48}O_{184}]^{33-}$ ($P_8W_{48}$) possessing good proton and electron reservoir abilities. The novel $P_8W_{48}$/rGO nanoassembly features excellent HER electrocatalytic performance as evidenced by the sustained production of hydrogen with a faradic yield of ca. 100%. Importantly, exceptionally low overpotentials are required for the HER (*e.g.* 28 mV at 10 mA cm$^{-2}$). The activity of $P_8W_{48}$/rGO is higher than those reported for the state-of-the-art precious metal-free electrocatalysts and compares well with that of the commercial Pt/Carbon (20 wt. % Pt). To our knowledge, this is the experimental evidence of the highest beneficial "microenvironment effect" on the HER electrocatalysis by a polyoxometalate.

**TOC entry**

A 3D configuration of reduced graphene oxide (rGO) nanosheets and a polyoxometalate $[H_7P_8W_{48}O_{184}]^{33-}$ ($P_8W_{48}$) possesses remarkable proton and electron reservoir abilities, showing significant hydrogen evolution activities at extremely low overpotential.
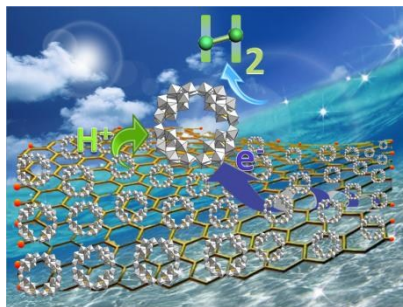
# Enhanced proton and electron reservoir abilities of polyoxometalate grafted on graphene for high-performance hydrogen evolution†

**Rongji Liu,[a] Guangjin Zhang,*[a] Hongbin Cao,[a] Suojiang Zhang,[a] Yongbin Xie,[a] Ali Haider,[b] Ulrich Kortz,*[b] Banghao Chen,[c] Naresh S. Dalal,*[c] Yongsheng Zhao,[d] Linjie Zhi,[e] Cai-Xia Wu,[f] Li-Kai Yan,*[f] Zhongmin Su[f] and Bineta Keita[g]**

[a]Key Laboratory of Green Process and Engineering, Institute of Process Engineering, Chinese Academy of Sciences, 100190, Beijing, China
E-mail: zhanggj@ ipe.ac.cn

[b]Jacobs University, Department of Life Sciences and Chemistry, P.O. Box 750 561, 28725 Bremen, Germany

E-mail: u.kortz@jacobs-university.de

[c]Florida State University, Department of Chemistry and Biochemistry, Tallahassee, FL 32306-4390, USA

E-mail: dalal@chem.fsu.edu

[d]Beijing National Laboratory for Molecular Sciences (BNLMS), Key Laboratory of Photochemistry, Institute of Chemistry, Chinese Academy of Sciences, 100190, Beijing, China

[e]Key Laboratory of Nanosystem and Hierarchical Fabrication, National Center for Nanoscience and Technology, 100190, Beijing, China

[f]Faculty of Chemistry, Northeast Normal University, 130024, Changchun, China

E-mail: yanlk924@nenu.edu.cn

[g]Retired from Université Paris-Sud, Laboratoire de Chimie-Physique, UMR 8000 CNRS, Orsay, F-91405, France.

## Abstract

A beneficial "microenvironment effect" on the efficiency of confined electrocatalysts is predicted by theory. However, examples of its experimental confirmation are scarce for catalysts based on polyoxometalates for the hydrogen evolution reaction (HER). For this purpose, the cyclic 48-tungsto-8-phosphate $[H_7P_8W_{48}O_{184}]^{33-}$ ($P_8W_{48}$) was fixed in a 3D configuration on reduced graphene oxide sheets (rGO) to boost it's HER activity. The HRTEM imaging and the solid state $^{31}P$ NMR spectrum of $P_8W_{48}$/rGO reveal a strong interaction between individual $P_8W_{48}$ and transparent rGO sheets. The calculation of the interaction between $P_8W_{48}$ and graphene (G) sheet is difficult to perform within a reasonable period of time because of the large size and very high overall negative charge of $P_8W_{48}$. However, as $P_8W_{48}$ is symmetrical, a quarter of its structure $[H_2P_2W_{12}O_{48}]^{12-}$ ($P_2W_{12}$) was extracted as a DFT calculation model. As $P_8W_{48}$ in $P_8W_{48}$/rGO is neutral that is surrounded by counter cations, the calculation model $P_2W_{12}$ is neutral with protons considering the affordable computational time. The adsorption energy for $P_2W_{12}$ on G (-1.55 eV) and the charge transfer between $P_2W_{12}$ and G (0.66 |e|) indicate that a strong interaction between $P_2W_{12}$ and G sheet exists. Kinetic study shows that the $P_8W_{48}$/rGO hybrids display excellent HER activity in acid; further confirmed by reproducible generation of hydrogen with quantitative faradaic yield and a high turnover frequency (11 s$^{-1}$ at 295 mV overpotential) for a noble metal-free electrocatalyst. Importantly, the overpotentials

required for the HER compare well with those of the commercial Pt/C (20 wt. % Pt), which indicates that $P_8W_{48}$/rGO is a promising cheap HER electrocatalyst. To our knowledge, this is the experimental evidence of the highest beneficial "microenvironment effect" on the HER electrocatalysis by a polyoxometalate.

## 1. Introduction

The effective generation of hydrogen from the electrolysis of water can be viewed as a promising solution to a clean energy carrier for the future.[1] The noble metals such as Pt have been utilized as the most efficient electrocatalysts for the hydrogen evolution reaction (HER) by water splitting. However, the high cost and shortage of Pt reserve limit its widespread use. Therefore, a great deal of effort is still needed for the replacement of Pt with more earth-abundant metals. Among Pt-free and very efficient HER catalysts, the exciting family of transition metal chalcogenides,[2] especially nanostructured $MoS_x$ ($x \approx 2$ to 3),[2a-g] have received significant attention. Most of these HER electrocatalysts are promising candidates for application in proton exchange membrane technology based electrolysis.

Polyoxometalates (POMs) are another vast class of well-defined, early transition metal-oxo clusters widely used as electrocatalysts for various challenging reactions including the HER.[3] The few very effective POM-based electrocatalysts for the HER in aqueous media were obtained with Kortz's polyanions $[Co_6(H_2O)_{30}\{Co_9Cl_2(OH)_3(H_2O)_9(\beta-SiW_8O_{31})_3\}]^{5-}$,[4a] and $[Cu^{II}_2Pd^{II}_{22}P^V_{12}O_{60}(OH)_8]^{20-}$,[4b] Dolbecq's organic-inorganic hybrid based on the $[\epsilon-PMo^V_8Mo^{VI}_4O_{36}(OH)_4Zn_4]$ POM building units,[4c] and the composite based on the classical 12-tungstophosphate $[PW_{12}O_{40}]^{3-}$ Keggin ion in combination with carbon nanotubes reported by Xu and co-workers.[4d] More recently, the Mo-derivative $[PMo_{12}O_{40}]^{3-}$ was used for successful water splitting by Cronin and co-workers;[4e] these authors reported also on highly efficient HER electrocatalysts based on $[SiW_{12}O_{40}]^{3-}$ associated to Pt.[4f] Qin and co-workers also reported recently on high-performance HER electrocatalysts based on polymolybdate and metal−organic frameworks.[4g] However, for an attractive alternative to precious metal-based HER electrocatalysts, facile and green synthesis in large scale of a cost-effective and efficient electrocatalyst still remains a challenge. In this respect, one of the approaches consists in the development of three-dimensionally distributed catalysts supported on high-surface-area conducting materials. Owing to the so-called "microenvironment effect", improvement of the activity of such immobilised electrocatalysts is expected, based on theoretical grounds.[5] The main advantages to be gained with these heterogeneous catalysts include the use of ultra-small amount of catalyst and the proximity of the catalyst and the electron source.

Most POMs are good candidates as HER electrocatalysts in homogeneous liquid phase thanks to their electron and proton reservoir behaviours. Indeed, most of them undergo fast and chemically reversible multi-electron processes which proceed through electrochemical and chemical processes in which the common chemical steps are protonations. However, their use as very effective HER heterogeneous electrocatalysts in water is restricted by several drawbacks including their high solubility, low surface area and the high overpotentials required to afford significant current densities. We have shown that the cyclic 48-tungsto-8-phosphate $[H_7P_8W_{48}O_{184}]^{33-}$ ($P_8W_{48}$) fixed on the carbon Vulcan XC-72 ($P_8W_{48}$/Vulcan) is significantly more efficient for the HER compared to $P_8W_{48}$ as homogeneous liquid phase electrocatalysts.[4a] It is worth noting that $P_8W_{48}$ is stable in a large pH domain and can undergo fast and chemically reversible multi-electron processes at remarkably favorable potentials in comparison with classical POMs. Cyclic voltammetry and confocal microscopy were used to demonstrate that the superior HER activity of $P_8W_{48}$/Vulcan is due to the improvement of its proton and electron reservoir-like abilities induced by the aforementioned "microenvironment effect" which enhances the basicity of $P_8W_{48}$.[4a] However, the HER activity of $P_8W_{48}$/Vulcan is by far less important than those reported for the best noble metal-free electrocatalysts. We also reported on different synthetic routes for the design of hybrids based on $P_8W_{48}$ and reduced graphene oxide

($P_8W_{48}$/rGO).[6] However, these hybrids did not present electrocatalytic activity towards the HER in the potential domain of interest in the present work.[6]

Herein we present a novel synthetic method for the preparation of hybrid nanomaterial based on $P_8W_{48}$/rGO as electrocatalyst for the HER in acidic aqueous solutions. The idea was to provide an experimental evidence of the predicted beneficial effect,[5] for the HER, which could result from the appropriate immobilization of a POM ($P_8W_{48}$) possessing good proton and electron reservoir abilities,[3o,4a] on rGO as an excellent conducting and large surface area support.[7] Indeed, our results confirm that the resulting $P_8W_{48}$/rGO hybrids with highly-dispersed $P_8W_{48}$ feature outstanding electrocatalytic performance towards the HER and compare well with that of the commercial Pt/C (20 wt. % Pt). To our knowledge, this is the experimental evidence of the highest beneficial "microenvironment effect" on the HER electrocatalysis by a polyoxometalate. Importantly, $P_8W_{48}$ is common and robust and can be prepared with a suitable method for mass production.

## 2. Experimental section

### 2.1. Materials

The potassium-Lithium salt of $P_8W_{48}$ ($K_{28}Li_5[H_7P_8W_{48}O_{184}] \cdot 92H_2O$) was synthesized according to the published procedure cited in the ref. 8: Briefly 8-g sample of $K_{12}H_2P_2W_{12}O_{48} \cdot 24H_2O$ was dissolved in 250 mL of 1 M lithium chloride acidified by 0.7 mL of glacial acetic acid. The solutions was left for 4 h at room temperature and then 50 mL of saturated potassium chloride was added. The white precipitate was filtered off and washed once with potassium chloride solution and twice with ethanol. The metatungstate $[H_2W_{12}O_{40}]^{6-}$ ($H_2W_{12}$) (Fluka, purum), Pt/C catalyst (nominally 20% platinum on high surface area advanced carbon support), Nafion membrane (N-117, 0.18 mm-thick), Pt gauze and glassy carbon (GC) plate were purchased from Alfa Aesar. Nafion 117 solution (~5% in a mixture of lower aliphatic alcohols and water) and hydrazine solution (35 wt. % in water) were purchased from Sigma Aldrich. Ammonia solution (25-28 wt. % in water) and Sulfuric acid were purchased from Beijing Chemical Works. All chemical reagents were used as received. The detailed redox behaviours of $P_8W_{48}$[3o] and $H_2W_{12}$[9] were already published. Ultrapure water purified with Milli-Q (MQ) plus system (Millipore Co.) with resistivity of 18.2 MΩ cm was exclusively used in all aqueous solutions and rinsing procedures.

Our criteria in the choice of the appropriate POMs were the use of common and stable POMs in the pH 0.3 medium which can be prepared with a suitable method for mass production. Moreover, among them, we had to select those possessing good proton and electron reservoir abilities to fulfil the operative "microenvironment effect" requirements. Based on these criteria and previous works reported by some of us (ref. 4a and refs. therein), $P_8W_{48}$ and $H_2W_{12}$ are the best candidates for this issue.

### 2.2. Synthesis of $P_8W_{48}$/rGO

GO was oxidized from natural graphite (NG) flakes by a modified Hummers method[10] using $H_2SO_4$, $NaNO_3$ and $KMnO_4$ in an ice bath.[11] The resulting homogeneous brown GO dispersion was tested to be stable for several months and used for reduction. In a typical synthesis, aqueous solution of $P_8W_{48}$ (15 mL, 1.6 mM) was mixed with aqueous solution of GO (15 mL, 0.6 mg mL$^{-1}$) under the assistance of sonication and stirring to form a homogeneous suspension, pH = 1.0 $H_2SO_4$ was used as the solvent. Controlled potential coulometry measurements were conducted in a three-electrode conventional glass cell with the mixed suspension of $P_8W_{48}$ and GO as the electrolyte solution. A glassy carbon (GC) plate was used as the working electrode, a saturated calomel electrode (SCE) was used as the reference electrode and a Pt gauze with large surface area was used as counter electrode (both the reference and counter electrodes were separated from the electrolyte by a glass frit). The electrolyte was saturated with ultrahigh-purity Ar for at least 30 min and kept under a positive pressure of this gas during the experiments. To fully reduce the $P_8W_{48}$ solution by 16 electrons ($P_8W_{48}$ (16 e$^-$)), a potential of - 0.65 V vs. SCE was set on the working electrode. The polyanion $P_8W_{48}$ ($[H_7P_8W_{48}O_{184}]^{33-}$) was obtained by dissolving the salt

$K_{28}Li_5[H_7P_8W_{48}O_{184}] \cdot 92H_2O$ in an acidic medium.[8] The 16-electron reduced form of $P_8W_{48}$ is $H_{16}[P_8W_{48}]$ because the electrochemistry of $P_8W_{48}$ undergoes fast and chemically reversible multi-electron processes which proceed through electrochemical and chemical processes in which the chemical steps are protonations.[3o] After the electrochemical reduction was completed, the cell with dark-blue suspension of $P_8W_{48}$/rGO was covered tightly and left to stand for several hours until the blue was disappeared. Then, the suspension was filtered with a Whatman membrane (pore size 220 nm) and washed thoroughly with ultrapure water for 3 times. Before further characterizations, the nanocomposites were dried in a vacuum oven at 80 ℃ for 48 h. The amount of $P_8W_{48}$ in the $P_8W_{48}$/rGO hybrid was calculated according to the Faraday's law by integration of the first 8-electron W reduction wave of $P_8W_{48}$/rGO. The influence of the concentration of $P_8W_{48}$ (16 e[-]) was studied by using 25 % and 50 % of the concentration used for the preparation of $P_8W_{48}$/rGO. These samples will be named as $P_8W_{48}$/rGO-25 and $P_8W_{48}$/rGO-50 respectively.

### 2.3.   Synthesis of $H_2W_{12}$/rGO

$H_2W_{12}$/rGO was prepared with the same method as that of $P_8W_{48}$/rGO. Typically, aqueous solution of $H_2W_{12}$ (26 mL, 3 mM) was mixed with aqueous solution of GO (4 mL, 0.6 mg mL^{-1}) under the assistance of sonication and stirring to form a homogeneous suspension, pH=1.0 $H_2SO_4$ was used as the solvent. Controlled potential coulometry measurements were conducted in a three-electrode conventional glass cell with the mixed suspension of $H_2W_{12}$ and GO as the electrolyte solution. The electrolyte was saturated with ultrahigh-purity Ar for at least 30 min and kept under a positive pressure of this gas during the experiments. To fully reduce the $H_2W_{12}$ solution by 4 electrons, a potential of - 0.615 V vs. SCE was set on the working electrode. After the electrochemical reduction was completed, the cell with dark-blue suspension of $H_2W_{12}$/rGO was covered tightly and left to stand for several hours until the blue was disappeared. Then, the suspension was filtered with a Whatman membrane (pore size 220 nm) and washed thoroughly with ultrapure water for 3 times. Before further characterizations, the nanocomposites were dried in a vacuum oven at 80 ℃ for 48 h.

### 2.4.   Synthesis of rGO-hydrazine

rGO-hydrazine was prepared according a slightly modified literature method.[12] Typically, to a glass vial with homogeneous GO dispersion (25 ml, 0.6 mg ml^{-1}), 30 μl of hydrazine solution (35 wt. % in water) and 210 μl of ammonia solution (25-28 wt. % in water) were added. The weight ratio of hydrazine to GO was about 7:10. After being stirred for a few minutes, the vial was put in a water bath (95 ℃) for 1 h, and the chemical reduction was completed. Being cooled down naturally, then the suspension was filtered with a Whatman membrane (pore size 220 nm) and washed thoroughly with ultrapure water for 3 times. At last, the nanocomposites were dried in a vacuum oven at 80 ℃ for 24 h before further electrochemical measurements.

### 2.5.   Sample Characterizations

The field-emission scanning electron microscopy (FESEM) analysis was performed on a Hitachi model S-4300 FESEM. Transmission electron microscopy (TEM) and high-resolution TEM (HRTEM) images were obtained using a JEM-2010 TEM at an acceleration voltage of 200 kV. X-ray photoelectron spectroscopy (XPS) measurements were performed in ultrahigh vacuum (UHV) with Krato, AXIS-HS monochromatized Al Kα cathode source, at 75-150 W, using low energy electron gun for charge neutralization. Raman spectra were obtained with a Renishaw Raman system model 1000 spectrometer. The 532-nm radiation from a 20-mW air-cooled argon ion laser was used as the exciting source. The laser diameter was 1 μm, and the laser power at the sample position was 4.0 mW. The data acquisition time was 10 s. Fourier transform infrared spectroscopy (FT-IR) patterns were measured in the range 400-4000 cm^{-1} on an Alpha Centauri FTIR spectrophotometer.

All solid-state NMR experiments were carried out at room temperature on a Bruker AVIII HD 500 MHz WB spectrometer operating at 11.74 T with a Bruker 4-mm WB CPMAS probe. The Larmor frequencies of $^{31}P$ is 201.54 MHz. The $^{31}P$ static and MAS NMR spectra of $P_8W_{48}$ and $P_8W_{48}$/rGO were collected by spinning at 0 and 12 kHz, respectively, after 256 and 1024 scans with a 1.5 µs pulse (corresponding to a nominal $90^o$ pulse length of 4.5 µs) and a 30 s recycle delay. To facilitate the MAS study of the conducting $P_8W_{48}$/rGO, the sample was homogeneously mixed with nonconductor filler (volume ratio 1:2) before spun in the magnetic field. The chemical shift of spectra was referenced to 85% $H_3PO_4$ at 0 ppm.

### 2.6.    Electrochemical experiments

**Preparation of the modified electrodes**. Typically, 3 mg of the finely ground catalyst ($P_8W_{48}$/rGO, $P_8W_{48}$/rGO-25, $P_8W_{48}$/rGO-50, $H_2W_{12}$/rGO, rGO-hydrazine or Pt/C) was dispersed in 1 ml of anhydrous alcohol (3 mg mL$^{-1}$) by at least 30 min sonication to form a homogeneous ink. Then 12.6 µl of the catalyst ink was loaded onto a GC rotating disk electrode (RDE) of 4 mm in diameter (the loading of catalysts was 0.3 mg cm$^{-2}$). After drying, the electrodes were further modified with a thin film of Nafion by dropping 1.0 µL 0.1wt. % Nafion solution (isopropanol as the solvent) onto its surface. At last, six electrodes modified with the $P_8W_{48}$/rGO/Nafion film, $P_8W_{48}$/rGO-25/Nafion film, $P_8W_{48}$/rGO-50/Nafion film, $H_2W_{12}$/rGO/Nafion film, rGO-hydrazine/Nafion film and Pt/C/Nafion film were prepared respectively.

**HER measurements.** The electrochemical set-up was a CHI 760E electrochemical workstation (CHI Instrument, Inc.). A standard three-electrode cell was used and was controlled at 25 $^o$C using a water bath during the experiment. The prepared thin film GC RDE was used as the working electrode. A Pt gauze or a GC plate was used as counter electrode, and a SCE was used as reference electrode, both were separated from the electrolyte by glass frit. The electrolyte, consisting of a solution of 0.5 M $H_2SO_4$ (pH=0.3), was saturated with ultrahigh-purity $H_2$ for 30 min before cyclic voltammetry (CV) and linear sweep voltammetry (LSV) measurements. The SCE was calibrated with respect to reversible hydrogen electrode (RHE) in all measurements. The calibration was performed in the high purity $H_2$ saturated electrolyte with both Pt wires as the working and counter electrode. CVs were run at a scan rate of 1 mV s$^{-1}$, and the average of the two potentials at which the current crossed zero was taken to be the thermodynamic potential for the hydrogen electrode reactions. In 0.5 M $H_2SO_4$ (pH=0.3), E (RHE) = E (SCE) + 0.265 V. All potentials, $E$, are quoted with respect to the RHE.

**Controlled potential electrolysis for $H_2$ production.** For the quantitative detection of faradaic yield of $H_2$ production, a two-compartment H-cell fitted with a fresh Nafion membrane was used. One compartment was equipped with a GC plate modified with the fully activated $P_8W_{48}$/rGO used as the working electrode and a SCE used as the reference electrode, the other was equipped with a GC plate with large surface area used as the counter electrode. For the preparation of modified GC plate working electrode, the catalyst ink of $P_8W_{48}$/rGO was fixed onto one side of the GC plate with an area of about 1 cm$^2$ (the loading of catalyst was 0.3 mg cm$^{-2}$), followed by dropping 10.0 µL 0.1wt. % Nafion solution. Controlled potential coulometry measurement was performed after the reduction potential was set. The evolved $H_2$ was analyzed by a gas chromatograph (TCD, molecular sieve 5A column, Ar as the carrier).

## 3.    Results and Discussion

**Synthesis, physical characterizations and DFT calculations.** Scheme 1 features the schematic preparation procedure of the one-step electrochemical reduction synthesis of $P_8W_{48}$/rGO nanocomposite. The elaboration of $P_8W_{48}$/rGO hybrids was performed by reaction of the 16-electron reduced form of $P_8W_{48}$ (abbreviated as $P_8W_{48}$ (16 e$^−$)) with GO in pH 1.0 sulphate medium. During this reduction process the electrons stored in $P_8W_{48}$ (16 e$^-$) are easily transferred to GO, leading to the reduction of GO into rGO and the recovery of $P_8W_{48}$. Based on previous report on the facile fixation of POMs including $P_8W_{48}$ on various surfaces,[4a,11,13] it is probable that the $P_8W_{48}$ clusters assemble on the surface of rGO sheets leading to $P_8W_{48}$/rGO hybrids.
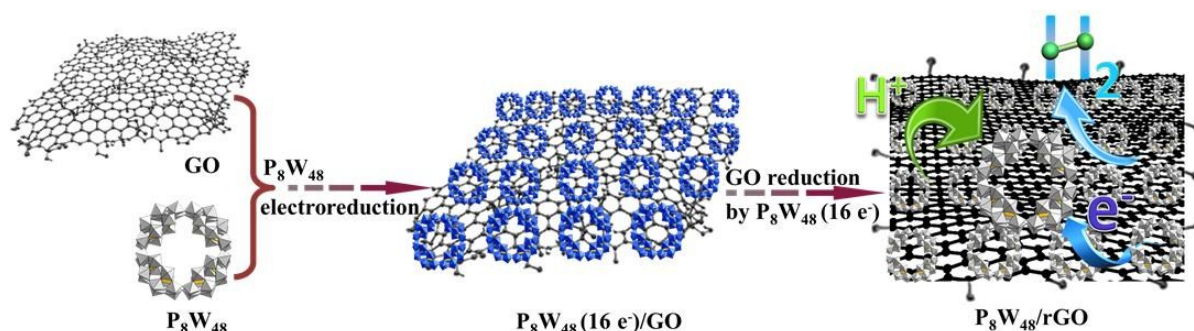
**Scheme 1** Schematic preparation procedure of the one-step electrochemical reduction synthesis of the $P_8W_{48}$/rGO nanocomposite.

Fig. 1a shows the typical FESEM image of the resulting $P_8W_{48}$/rGO nanocomposite. It can be clearly observed that large-scale rGO sheets with so many crumpled silk veil waves, something like tremella, were successfully obtained, indicating the efficient reduction of GO. The energy-dispersive X-ray spectrum (EDS) elemental mapping images (Fig. S1, ESI†) on carbon, oxygen, phosphorus and tungsten demonstrate the homogeneous distribution of $P_8W_{48}$ clusters on the surface of rGO sheets. The oxygen mainly comes from the residual oxygen containing groups in rGO and also the combining oxygen in $P_8W_{48}$. Meanwhile, typical TEM (Fig. 1b and Fig. 1c with different magnifications) and HRTEM (Fig. 1d) images illustrate that so many nanoclusters with the diameter of about 2 nm are uniformly dispersed on transparent rGO nanosheets. It should be noted that the diameter of $P_8W_{48}$ cluster based on terminal oxygens on opposite sides of the ring is 2.2 nm determined from crystallographic data. Thus it unambiguously reveals that the nanoclusters are attributable to $P_8W_{48}$.
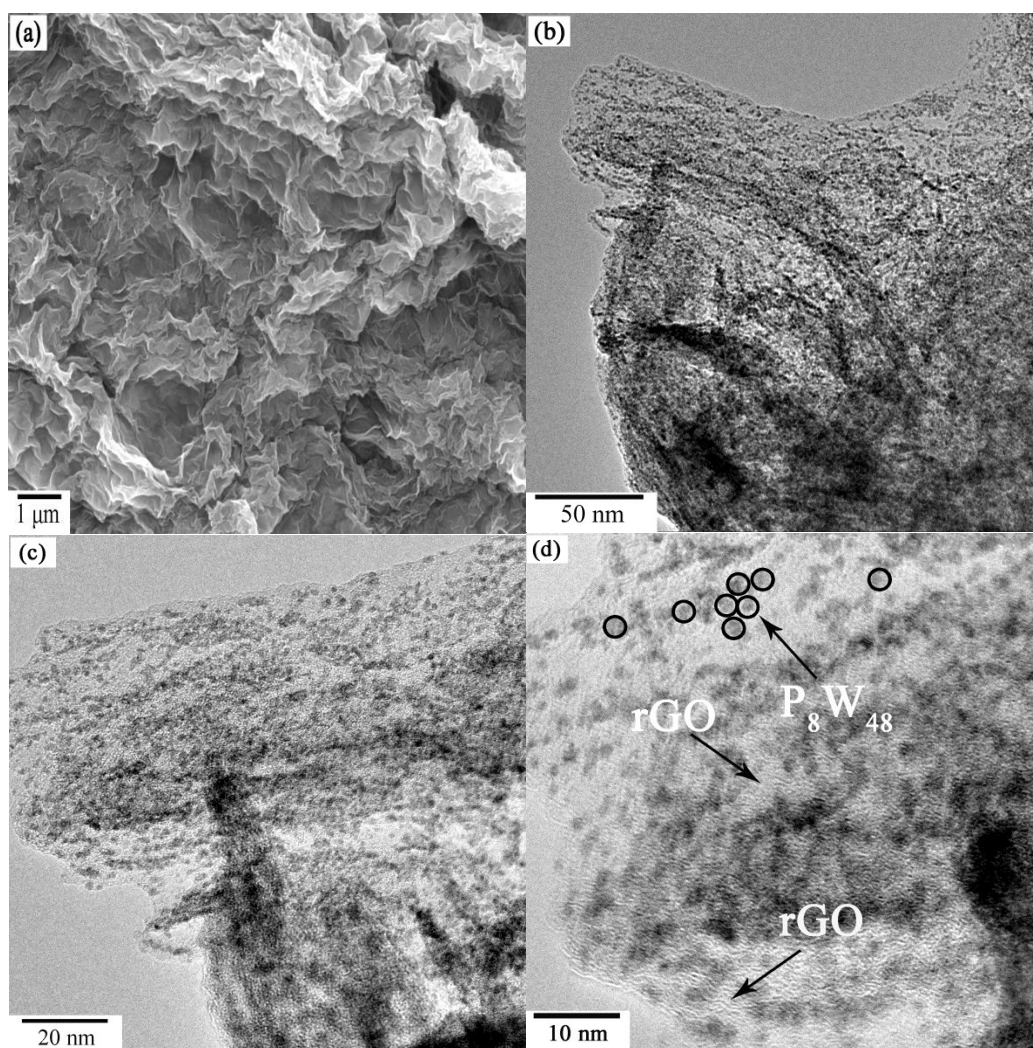
**Fig. 1** (a) FESEM, (b) and (c) different magnifications of TEM and (d) HRTEM images of the as-prepared $P_8W_{48}$/rGO nanocomposite.

The nanocomposite was further characterized by XPS, Raman spectroscopy and FT-IR. The details were shown in Supplementary Section SI-(1-3), Fig. S (2-4), Table S1 and Table S2 (ESI†). The XPS and Raman results indicate that the electrochemical reduction can greatly decrease the amount of the oxygen containing groups on GO while significant $sp^3/sp^2$ - hybridized carbon structures are restored. The XPS and FT-IR results suggest that the intact $P_8W_{48}$ is still there in the $P_8W_{48}$/rGO nanocomposite, and a strong interaction exists between the rGO sheets and the grafted, intact $P_8W_{48}$ nanoclusters.

It is well-known that polyoxometalates tend to spontaneously adsorb onto different carbon materials including graphene (G).[11,13] This adsorption is attributed to an electrostatic interaction which proceeds through proton transfer from the polyoxometalates to the oxygen-containing groups present on these materials. Recent DFT studies reported by some of us demonstrate that the interaction of the polyoxometalate $[PW_{12}O_{40}]^{3-}$ ($PW_{12}$) and graphene is noncovalent and that the formation of the $PW_{12}$/G hybrid involves electron transfer from $PW_{12}$ to graphene.[14] In agreement with such observation, our XPS results reveal that the $W^{VI}$ 4f peaks of the $P_8W_{48}$/rGO nanocomposite shift to lower binding energies compared with those of $P_8W_{48}$ (Fig. S2c, e and Table S2, ESI†), which suggests the electron transfer from $P_8W_{48}$ to rGO decreasing the electronegativity of the adjacent terminal oxygen atoms of $P_8W_{48}$. Therefore, the interaction between $P_8W_{48}$ and rGO could be due, at least partly, to a noncovalent adsorption process because the XPS observations show that the amount of the oxygen-containing groups of rGO is small compared to that of GO. The calculation of the interaction between $P_8W_{48}$ and graphene sheet is difficult to perform at the affordable time because $P_8W_{48}$ possesses large scale and very high overall negative charge. Therefore, a quarter of structure $P_8W_{48}$ ($P_2W_{12}$) was extracted as a calculation model as $P_8W_{48}$ is symmetrical. The interaction between $P_2W_{12}$ (neutral and anionic) and graphene was investigated based on DFT calculations by using the SIESTA (Spanish Initiative for the Electronic Simulations of Thousand of Atoms) program package.[15] The geometry and energy properties were described using general gradient approximation (GGA) in the scheme of Perdew−Burke−Ernzerhof (PBE),[16] and the double-ξ basis set plus polarization (DZP) function was used for all elements. The cut-off energy of the plane-wave basis is 200 eV, and $3 \times 3 \times 1$ k-point meshes were used for the Brillouin zone integration. The atomic relaxation is carried out until forces are less than 0.1 eV/Å, while the energy properties were carried out until forces are less than 0.02 eV/Å. In the $P_2W_{12}$/G structure, the orthogonal cells $24.60 \times 25.56 \times 30.00$ Å with 240 carbon atoms are used (Scheme 2).



**Top View**          **Side View**
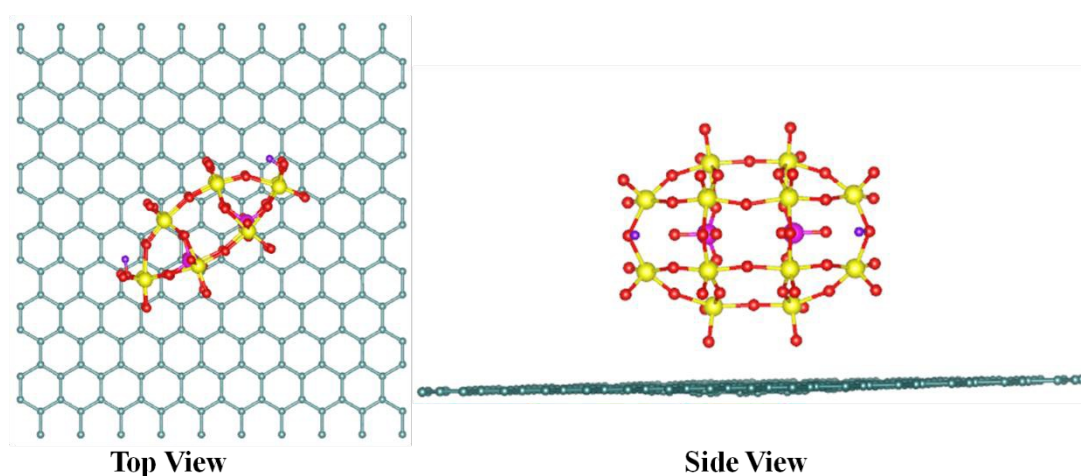
**Scheme 2** The most stable optimized structure for $P_2W_{12}$/G. Color code: W (yellow), O (red), P (pink), C (green), H (violet).

To investigate the affinity between POM and the graphene, we define the adsorption energy as:

$$E_a = E_{G-POM} - E_G - E_{POM}$$

where $E_{G-POM}$, $E_{POM}$, and $E_G$ stand for the total energies of the $P_2W_{12}$/G complex, the free $P_2W_{12}$, and the isolated graphene sheet, respectively. The adsorption energy for neutral $P_2W_{12}$ on graphene sheet in our calculations is -1.55 eV, indicating that the adsorption process of $P_2W_{12}$ on graphene is strong chemical adsorption. The same results can also be drawn from the charge transfer, that is, the charge transfer between $P_2W_{12}$ and graphene is 0.66 |e|, indicating that the strong interaction between $P_2W_{12}$ and the graphene sheet exists. Furthermore, the vertical distance d (calculated as the average z coordinate of atoms in the interfacial) of POM above the surface is 2.16 Å, which is within the sum range of van der Waals radii of related interfacial atoms. As expected, the adsorption energy (-38.53 eV) and charge transfer (5.43 |e|) for the anionic $P_2W_{12}$ ($[H_2P_2W_{12}O_{48}]^{12-}$) are much larger than that obtained with the neutral $P_2W_{12}$ model. It is worth noting that the adsorption energy (-0.36 ~ -1.79 eV according to six different configurations) and charge transfer (0.18 ~ 0.24 |e|) reported on the interaction between the polyanion $[PW_{12}O_{40}]^{3-}$ and graphene are strikingly smaller compared to those of $[H_2P_2W_{12}O_{48}]^{12-}$.[14] This observation underscores the strong interaction between $P_2W_{12}$ and graphene.

Even more direct evidence for the stability of $P_8W_{48}$ as an intercalated molecule in graphene, and also for strong perturbation of its molecular orbitals by the substrate graphene is seen via ^{31}P-NMR of essentially the same samples as used for catalytic studies. We surmised that ^{31}P-NMR isotropic chemical shift will be sensitive to change in the electronic density distribution in the P orbitals due to any chemical bonding with rGO. The obtained data indeed provide a clear evidence of electronic communication between $P_8W_{48}$ and rGO. The static ^{31}P spectrum of $P_8W_{48}$ (Fig. 2a/top) shows a typical powder pattern (asymmetry parameter $\eta$ = 0.94, less than axial symmetry, $\delta_{iso}$ = -8.3 ppm), showing that the broadening is due to chemical shift anisotropy, CSA. However, the line-shape of static NMR of $P_8W_{48}$/rGO (Fig. 2a/bottom) is a "broad featureless hump" due to the overlapping of many powder patterns as well as the interplay of the different broadening mechanisms, indicating the local environment changes around ^{31}P after being absorbed on the surface of graphene, especially with the highly delocalized unpaired electron of rGO.
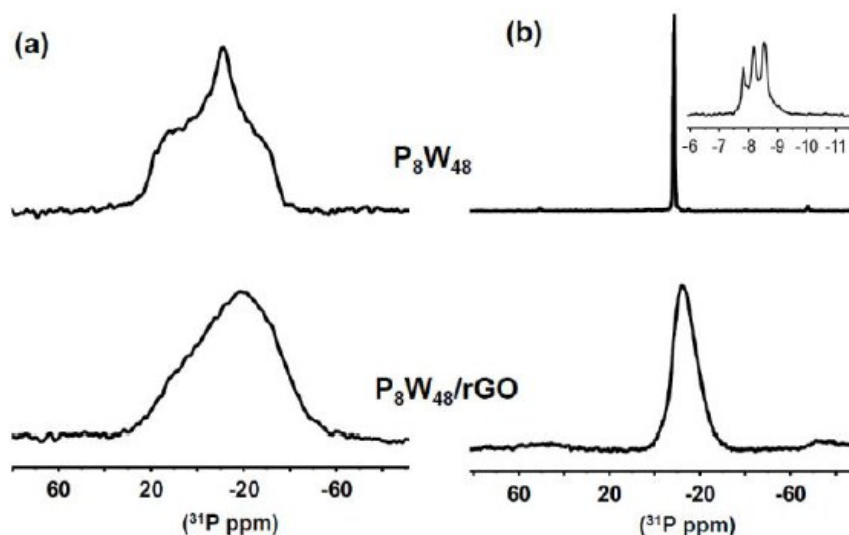


**Fig. 2** (a) Static and (b) MAS ^{31}P NMR spectras of $P_8W_{48}$ (top) and $P_8W_{48}$/rGO (bottom).

The ^{31}P MAS spectrum (Fig. 2b/top) of $P_8W_{48}$ clearly exhibits three sharp resonances at -7.8, -8.3 and -8.6 ppm, indicating the existence of three magnetically inequivalent P nuclei in the polyanion structure; it reflects the local asymmetry around the polyanion in solid state before being introduced into the $P_8W_{48}$/rGO nanocomposite.[8,17,18] On the other hand, only one broad resonance centered at -12 ppm with a half width of 2.3 kHz (though much narrower than that of the static

experiment, 9.5 kHz) is present in the $^{31}$P MAS spectrum of $P_8W_{48}$/rGO (Fig. 2b/bottom). This huge line broadening and a large shift points directly to a distribution of local environments around the P atoms caused by strong interaction between $P_8W_{48}$ and rGO which can't be removed by high speed MAS. These results fully support a strong interaction between $P_8W_{48}$ and rGO and also $P_8W_{48}$'s essential stability in rGO.

**Electrochemistry and hydrogen evolution reaction electrocatalysis.** Owing to its insolubility, the electrochemistry of $P_8W_{48}$/rGO was performed in the solid-state by entrapping it in a perfluorinated polymer (Nafion). The experiments were carried out in a pH 0.3 sulphate medium at a GC RDE electrode. CV was used to probe the basicity of the reduced form of $P_8W_{48}$ because it is well-known that its electrochemistry undergoes fast and chemically reversible multi-electron processes which proceed through electrochemical and chemical processes in which the common chemical steps are protonations.[3o] The change of basicity of $P_8W_{48}$ is featured on the Fig. 3 which compare the CV characteristics of $P_8W_{48}$/rGO with those of $P_8W_{48}$ dissolved in the same medium. Fig. 3a exhibits the superimposed representative CV patterns of $P_8W_{48}$/rGO and $P_8W_{48}$ restricted to the 8-electron W wave. The current of $P_8W_{48}$ was scaled up to make its peak current match that of $P_8W_{48}$/rGO. In contrast with the CV of $P_8W_{48}$, that of $P_8W_{48}$/rGO shows a composite and quasi-reversible reduction wave (at ~ + 0.56 V versus RHE) which is attributed to the quinone-like moieties existing on rGO.[19] This redox process is followed by the first reversible reduction-wave of the W$^{VI}$ centers within $P_8W_{48}$/rGO (at + 0.11 V versus RHE). Strikingly, it appears that with $P_8W_{48}$ confined in the rGO sheets, a single 8-electron W wave is observed in place of the two 4-electron waves of $P_8W_{48}$ in solution which means that the reduced forms of $P_8W_{48}$/rGO are more basic because the protonation processes are easier (Fig. 3a). This phenomenon is attributed to the predicted "microenvironment effect" which is also observed on the other waves of $P_8W_{48}$/rGO (Fig. 3b). Consequently, the CV of $P_8W_{48}$/rGO exhibits a large HER wave in a potential domain where $P_8W_{48}$ is inactive for this reaction (inset in Fig. 3b). The remarkable increase of the $P_8W_{48}$ basicity induced by this beneficial effect boosts both protonation and electron transfer processes associated with $P_8W_{48}$ and accordingly the HER. Keita and co-workers reported such phenomenon for various POMs entrapped in carbon or polymer films.[4a,20] To assess whether this observation is due to the "microenvironment effect" on basicity, these authors resorted to confocal microscopy and demonstrated that, in the presence of different POMs including $P_8W_{48}$, the pH of the inside of the film is significantly higher compared to that of the bathing medium. In agreement with electrochemistry, confocal microscopy results confirm that the extent of the basicity increase depends strongly on the nature of the POM. However, the extent of this beneficial "microenvironment effect" on $P_8W_{48}$/rGO redox properties is by far higher than those reported for hybrids based on $P_8W_{48}$ on various supports.[4a,6] Moreover, the W reduction process occurs at more favorable potential (by ~0.060 V) for $P_8W_{48}$/rGO compared to $P_8W_{48}$ which reveals the expected advantages of rGO. Fig. S5a (ESI†) features the CV of 8-electron W wave as a function of the scan rate. As expected, both the linear characteristic symmetrical shape for the $P_8W_{48}$/rGO waves and the linear variation of its peak currents with the scan rate confirm that $P_8W_{48}$ is successfully grafted on rGO sheets (Fig. S5b, ESI†). In addition, the remarkable reproducibility of the CV characteristics over 1000 cycles underscores the stability of the $P_8W_{48}$/rGO modified electrodes in solution phase (Fig. S6, ESI†). Altogether, these electrochemical characteristics suggest that the $P_8W_{48}$/rGO hybrids are potentially good candidate for the HER. The CV pattern of $P_8W_{48}$/rGO between +0.715 V and +1.065 V versus RHE (Fig. S7, ESI†) features a typical quasi-rectangular shape indicating pure electrical double layer capacitor behaviour. Fig. S8 (ESI†) shows that this rectangular shape is not significantly distorted when increasing the potential scan rate from 10 to 200 mV s$^{-1}$. Furthermore, waves of the quinone-like moieties and the W centers are also not distorted at these scan rates (Fig. S9, ESI†). Finally, Fig. S10 (ESI†) shows that the surface area of the rGO in the $P_8W_{48}$/rGO hybrid is higher compared to that obtained via hydrazine assisted reduction of GO (rGO-hydrazine). These observations underline the high quality of the rGO component of the hybrids $P_8W_{48}$/rGO.
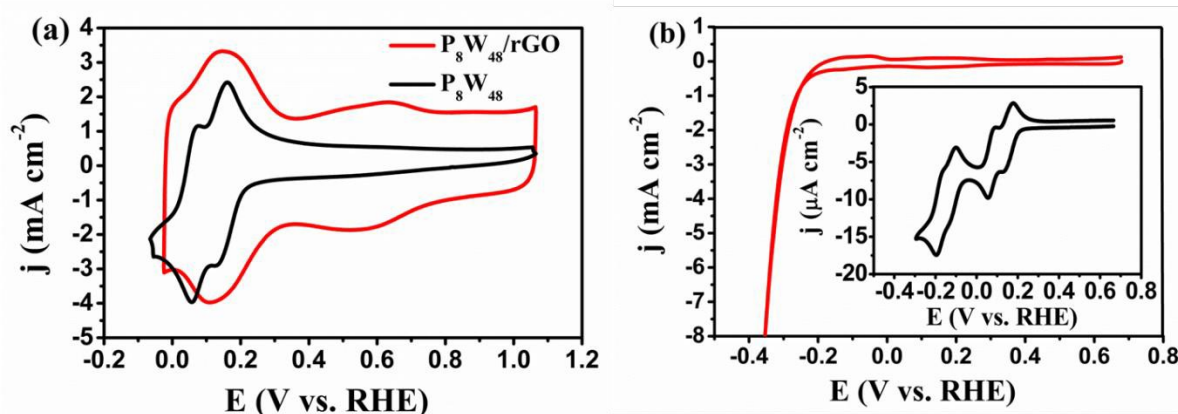
**Fig. 3** (a) Comparison of representative cyclic voltammograms of $P_8W_{48}$/rGO modified GC electrode (the catalyst loading was 0.3 mg cm$^{-2}$) and $P_8W_{48}$ (0.1 mM $P_8W_{48}$ in 0.5 M $H_2SO_4$) restricted to the first 8-electron W wave in the negative potential domain at a scan rate of 100 mV s$^{-1}$ and (b) the initial cyclic voltammogram of $P_8W_{48}$/rGO modified GC electrode which features the HER characteristics. The inset is the cyclic voltammogram of 0.1 mM $P_8W_{48}$ in 0.5 M $H_2SO_4$. The scan rate was 2 mV s$^{-1}$.

Strikingly, the second reduction wave (at -0.127 V versus RHE) of $P_8W_{48}$/rGO is followed closely by an irreversible and large current intensity wave attributed to the HER (Fig. 3b). In contrast, the inset in Fig. 3b shows that, on the bare GC electrode, the CV of $P_8W_{48}$ in solution does not feature a HER wave in the explored potential domain. Such observations underscore a huge "microenvironment effect" for the other waves of $P_8W_{48}$/rGO. As expected from our previous report on $P_8W_{48}$/Vulcan,[4a] the CV of $P_8W_{48}$/rGO features an improvement in the onset potential location of the HER upon cycling between + 0.665 V and - 0.4 V versus RHE and concomitantly gas bubbles are generated. Finally, the HER onset potential and current intensity no longer changes after 87 cycles. Fig. 4a presents the improvement of the characteristics of the HER wave during the first scans in order to highlight the early stages of this process. Such phenomenon was also observed by setting the potential at a value more negative than that of the second W-reduction wave (-0.127 V versus RHE); in other words in the HER potential domain. As expected, a steady increase of the HER current is also observed during the electrode activation with this potentiostatic method. For both methods the activation process was observed with either Pt or GC as the counter electrode. However, attention should be paid that when Pt is used as the counter electrode, and there are chlorides impurities in the electrolyte, Pt counter electrode dissolution will happen and thus the Pt deposition on the working electrode, which will increase the HER current and will make wrong estimation of the real catalytic activities of the catalysts. As a result, Pt impurity was detected in the $P_8W_{48}$/rGO film when the experiment was performed in the presence of 5 mM HCl because of the Pt counter electrode dissolution favored by the chlorides (see Supplementary Section SI-4 and Fig. S11, ESI†). Fig. S11a (ESI†) features the CVs of the resulting tricomponent Pt-$P_8W_{48}$/rGO and $P_8W_{48}$/rGO in superposition. Both CVs exhibit the first W redox couple, however that of Pt-$P_8W_{48}$/rGO presents, as expected, two additional waves, one on the forward and the other on the reverse potential scans. These waves are attributed, respectively, to the HER on the Pt nano-objects and the oxidation of the resulting hydrogen (at + 0.02 V versus RHE). Fig. S11b (ESI†) shows that the CV pattern of Pt/C features also such waves in the same potential domain. It is rewarding that trace amounts of Pt contaminant in a $P_8W_{48}$/rGO film can be easily detected by CV. Furthermore, owing to its high stability, Pt-$P_8W_{48}$/rGO should be a good candidate as an ultra-low Pt loading catalyst for various challenging reactions.

In the following, fully activated electrodes obtained with the potential cycling method were used for quantitative characterization the $P_8W_{48}$/rGO activity towards the HER. LSV was used to evaluate the electrocatalytic activity of the stable modified electrode towards the HER and compare it to those observed for $H_2W_{12}$/rGO (obtained with the POM $[H_2W_{12}O_{40}]^{6-}$), rGO-hydrazine, the commercial Pt/C (20 wt. % Pt) and the bare GC used as a support for all these electrocatalyst films. Our

criteria in the choice of the two POMs used here are based on previous reports on the "microenvironment effect" (the criteria are provided in experimental section 2.1). The mass loading for each sample was 0.3 mg cm$^{-2}$. The LSVs were used to carry out Tafel analysis for a quantitative comparison of their kinetic parameters i.e. exchange current densities ($i_0$) and Tafel slopes (b). The current density (i) in the Tafel equation ($\eta = a + b \log i$, where $\eta$ is the applied overpotential) was expressed in Ampere per unit of geometric surface area of the electrode. It is worth noting that, only the low overpotential domain was used for the Tafel analyses performed for the different systems. Fig. 4b illustrates a representative LSV obtained with P$_8$W$_{48}$/rGO and the corresponding Tafel polarization curve. Strikingly, exceptionally low overpotentials of 28, 39 and 70 mV are required to reach the HER current densities of 10, 20 and 50 mA cm$^{-2}$ respectively for P$_8$W$_{48}$/rGO which represents the best performance for the HER in aqueous media observed with noble metal-free electrocatalysts based on POMs. In comparison, a much higher overpotential (188 mV) was observed for H$_2$W$_{12}$/rGO at current density of 10 mA cm$^{-2}$ (Fig. 4c). Fig. 4c shows also that the HER activities of the bare GC and rGO-hydrazine are very low compared to those of P$_8$W$_{48}$/rGO. Moreover, the overpotential value for P$_8$W$_{48}$/rGO hybrid compares favourably with those obtained with effective noble metal-free electrocatalysts (Table 1 and Table S3 (ESI†)). Importantly, Fig. 4c even reveals that the HER electrocatalytic performance of P$_8$W$_{48}$/rGO compares well with that of Pt/C. For example, Pt/C requires a slightly larger overpotential (100 mV) than P$_8$W$_{48}$/rGO (70 mV) to achieve a current density of 50 mA cm$^{-2}$. It is worth noting that, under similar experimental conditions, the HER overpotentials for Pt/C are in agreement with reported results. For example, at an HER overpotential of 50 mV, the current density obtained with Pt/C (20.6 mA cm$^{-2}$) is close to that observed by Li and co-workers (20 mA cm$^{-2}$).[2d] The P$_8$W$_{48}$/rGO hybrid exhibits also remarkably low Tafel slope of ca. 38 mV per decade and exchange current density of ca. 2 mA cm$^{-2}$. This Tafel slope suggests a Volmer–Heyrovsky HER mechanism. As expected, the Tafel slope (84 mV per decade) and exchange current density (0.06 mA cm$^{-2}$) observed for H$_2$W$_{12}$/rGO confirm its lower HER activity compared to that of P$_8$W$_{48}$/rGO (Fig. S12, ESI†). It is worth noting that no significant decay of the modified electrode activity was observed after several days of storage in air saturated electrolyte or upon potential cycling for several hours per day for weeks. For example, after 1000 continuous cycles, only a slight decrease of the current density was observed (Fig. 4d). Altogether these observations underscore the excellent activity of P$_8$W$_{48}$/rGO towards the HER compared to those reported for precious metal-free electrocatalysts (Table 1 and Table S3 (ESI†)).

We attribute the superior performance of P$_8$W$_{48}$/rGO to the fact that it meets the main requirements for sustained electrochemical hydrogen production via heterogeneous catalysis *i.e.* efficient electron uptake and release from P$_8$W$_{48}$ in a potential domain close to the thermodynamic potential of the HER and fast and sustained protons supply to the reducing centers. The role of the "microenvironment effect" is crucial because it favours both proton and electron accumulation on the framework of P$_8$W$_{48}$ which boosts the HER. In other words, owing to this effect the protonation of the species P$_8$W$_{48}$/rGO is easier than that of P$_8$W$_{48}$ in solution and accordingly the electron transfer processes associated with P$_8$W$_{48}$/rGO, in agreement with previous reports.[4a,20] However, altogether the experimental observations reported in the present work and in previous studies about P$_8$W$_{48}$ fixed on rGO[6] or other supports[4a] suggest that the following features must be controlled to get outstanding "microenvironment effect" on the HER electrocatalysis: (i) the high basicity of P$_8$W$_{48}$ compared to those of most polyoxometalates of interest for the HER is a very important parameter because for weakly basic polyoxometalates the "microenvironment effect" is operative only if a very strong acidic medium is used as bathing electrolyte[20] (for example for the hybrids obtained with one of the less basic POM PW$_{12}$ confined on the carbon Vulcan XC-72, the "microenvironment effect" was not observed in the 0.5 M H$_2$SO$_4$ medium used in the present work[4a] in accordance with a previous report on PW$_{12}$/polymers hybrids which demonstrates that the observation of the "microenvironment effect" necessitates proton concentration as high as 5 M[20]); (ii) the high dispersion of individual P$_8$W$_{48}$ molecules on the rGO sheets favours the "microenvironment effect", indeed, this effect is low for layers of polyoxometalates unevenly distributed on various supports;[20] (iii) the uniform distribution of P$_8$W$_{48}$ was obtained thanks to the novel synthetic route used in the present that is more convenient for this issue than the reported methods;[6] (iv) the rGO sheets have also a beneficial influence because they act both as a highly conductive and convenient support for the preparation of three-dimensionally distributed and strongly

adsorbed $P_8W_{48}$ molecules which are among the main requirements for operative "microenvironment effect". Moreover, it is well-known that the reduced forms of polyoxometalates possess electron and proton transfer and/or storage abilities.[3b] However, unlike $P_8W_{48}$, the overpotentials required for the HER electrocatalysis by most polyoxometalates remain high. Therefore, the excellent activity of $P_8W_{48}$/rGO towards the HER is attributed to the "microenvironment effect" which enhances greatly the beneficial synergistic effect of $P_8W_{48}$ and rGO.

Although the reduction of GO by $H_2W_{12}$ is effective, the efficiency of the resulting $H_2W_{12}$/rGO is ca.108 times lower than that of $P_8W_{48}$/rGO which underscores the importance of $P_8W_{48}$ properties. The excellent electron transfer properties of the rGO are also beneficial for the HER because b and $i_0$ of $P_8W_{48}$/Vulcan[4a] are respectively more than 3 times higher and 4 times lower than those of $P_8W_{48}$/rGO. Moreover, as indicated above, the performance of rGO-hydrazine alone is insignificant with respect to $P_8W_{48}$/rGO (Table S3). It is worth noting that the high performance of $P_8W_{48}$/rGO was obtained with a very small loading ($4.179 \times 10^{-9}$ mol cm$^{-2}$) of $P_8W_{48}$ (the amount of $P_8W_{48}$ was calculated according to the Faraday's law by integration of the first 8-electron W reduction wave of $P_8W_{48}$/rGO. Indeed, it has been widely reported that the cyclic voltammograms of $P_8W_{48}$ solution or entrapped on various carbon materials including rGO present a first redox process featured by two closely separated four-electron W-waves or a single 8-electron W-wave as illustrated on the Fig. 3a.[3o,4a,6,8] Moreover, we have performed, IR, HRTEM and solid state NMR characterizations of the $P_8W_{48}$/rGO nanocomposite which reveal that individual $P_8W_{48}$ are strongly adsorbed on the rGO nanosheets. Therefore the amount of $P_8W_{48}$ in the $P_8W_{48}$/rGO hybrid can be calculated by using the first 8-electron W reduction wave of $P_8W_{48}$/rGO). To the best of our knowledge, there is only one report on a preliminary test of POM/rGO hybrids based on the POM $K_{12.5}Na_{1.5}$ [$NaP_5W_{30}O_{110}$], rGO and poly(ethylenimine) (PEI/$P_5W_{30}$-rGO)$_n$ as HER electrocatalyst (Table S3).[3p] The CV characteristics of the wave attributed to the HER show that the activity of (PEI/$P_5W_{30}$-rGO)$_n$ is much lower than that of $P_8W_{48}$/rGO as evidenced by the corresponding HER onset overpotential which is higher (by ca. 280 mV).
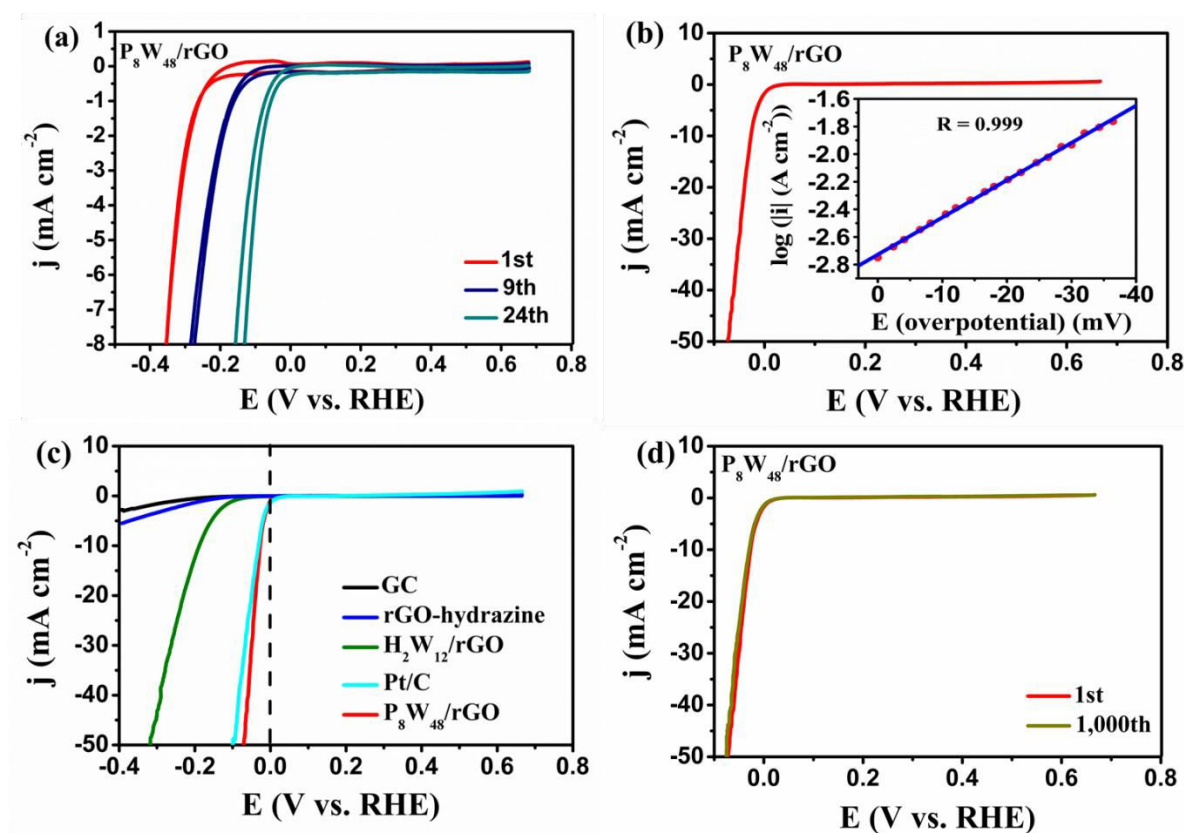
**Fig. 4** (a) The variation of the cyclic voltammogram characteristics of $P_8W_{48}$/rGO during the cycling, (b) Polarization curve (LSV curve) of $P_8W_{48}$/rGO, the inset is the corresponding Tafel plot obtained from the polarization curve, (c) comparison of the polarization curves obtained with several catalysts as indicated and (d) catalyst stability tests for $P_8W_{48}$/rGO in 0.5 M $H_2SO_4$ initially and after 1000 CV sweeps between +0.20 and −0.30 V vs RHE at a scan rate of 100 mV s$^{-1}$. The catalyst loading was 0.3 mg cm$^{-2}$. The scan rates of CV and LSV tests were 2 mV s$^{-1}$ and 5 mV s$^{-1}$ respectively.

**Table 1** Comparison of HER activity measured for $P_8W_{48}$/rGO with that reported for other effective systems under acidic conditions (0.5 M $H_2SO_4$).

| Catalyst | Loading (mg cm$^{-2}$) | Electrode | Current density (mA cm$^{-2}$) | Overpotential (mV vs. RHE) | Exchange current density (A cm$^{-2}$) | Tafel slope (mV dec$^{-1}$) | Ref. |
|---|---|---|---|---|---|---|---|
| **$P_8W_{48}$/rGO** | 0.3 | Glassy carbon | 10 | 28 | $2\times10^{-3}$ | 38 | **This work** |
| | | | 20 | 39 | | | |
| | | | 50 | 70 | | | |
| MoS$_2$/rGO | 0.28 | Glassy carbon | 10 | ~150 | N/A | 41 | 2d |
| 1T-WS$_2$ nanosheets | 1.0±0.2 | Graphite disk | 10 | 142 | N/A | 70 | 21 |
| [Mo$_3$S$_{13}$]$^{2-}$ clusters | 0.01-0.1 | Graphite paper | 10 | 180-220 | N/A | 38-40 | 2j |
| CoP | 2 | Ti foil | 20 | 85 | $1.4\times10^{-4}$ | 50 | 22 |
| MoP\|S | 3 | Ti foil | 10 | 64 | $5.7\times10^{-4}$ | 50 | 2h |
| | | | 20 | 78 | | | |
| | | | 100 | 120 | | | |

As the reduction degree of GO may influence the HER performance of $P_8W_{48}$/rGO, we also studied the influence of the concentration of $P_8W_{48}$ (16 e$^-$) by preparing another two samples $P_8W_{48}$/rGO-25 and $P_8W_{48}$/rGO-50 obtained respectively with 25 and 50% of the concentration of $P_8W_{48}$ (16 e$^-$)) used for $P_8W_{48}$/rGO. The electrocatalytic HER performance of these samples were investigated. Fig. S13 (ESI†) shows the XPS spectra of these two composites. It can be clearly observed from the C1s spectra (Fig. S13a, d and Table S1, ESI†) that the C-O contents of these two composites were different, indicating the different reduction degree of GO ($P_8W_{48}$/rGO-50 was reduced deeper than $P_8W_{48}$/rGO-25). Besides, the presence of tungsten in its full oxidation form (W$^{VI}$) and phosphorus (Fig. S13b, c, e and f, ESI†) were also detected, and the W$^{VI}$ 4f peaks of both samples shift to lower binding energies compared with those of pure $P_8W_{48}$ (Table S2, ESI†). Then the HER performance of these two samples was studied and compared with that of $P_8W_{48}$/rGO. Fig. S14a (ESI†) features the 10th cyclic voltammogram of each catalyst modified GC electrode which features the HER characteristics. It reveals that the $P_8W_{48}$/rGO-25 and $P_8W_{48}$/rGO-50 exhibit similar electrocatalytic activities toward HER, while the $P_8W_{48}$/rGO shows better electrocatalytic HER activity with lower overpotential due to the deep reduction degree of GO. Thus it unambiguously reveals that the reduction degree of GO is important for HER. Further, we investigated the activation process of the $P_8W_{48}$/rGO-25 modified electrode upon cycling between + 0.665 V and - 0.4 V versus RHE (Fig. S14b, ESI†). Interestingly, a steady increase of the HER current was also observed until saturation during the electrode activation with the potential cycling method. For fully activated electrodes, low overpotentials of 31, 52 and 109 mV are required to reach the HER current densities of 10, 20 and 50 mA cm$^{-2}$ respectively. It indicates that although the incompletely reduced GO was used as the catalyst support, the fully activated $P_8W_{48}$/rGO-25 electrode still exhibits high-performance electrocatalytic HER activity. It is attributed to the fact that rGO-25 can be further reduced to rGO during potential cycling, in combination with the well-suited partner $P_8W_{48}$.

The effect of the loading amount of $P_8W_{48}$ on the performance of HER has also been studied. Fig. S15a (ESI†) indicates the 10th cyclic voltammograms of $P_8W_{48}$/rGO modified GC electrodes which feature the HER characteristics with catalyst loading amount of 0.01, 0.05, 0.1, 0.2 and 0.3 mg cm$^{-2}$ respectively. The loading amount of $P_8W_{48}$ in each electrode was $1.393 \times 10^{-10}$, $6.965 \times 10^{-10}$, $1.393 \times 10^{-9}$, $2.786 \times 10^{-9}$ and $4.179 \times 10^{-9}$ mol cm$^{-2}$ respectively. It shows that the HER performance was improved sharply with the increasing of the loading amount of $P_8W_{48}$ until it comes to $1.393 \times 10^{-9}$ mol cm$^{-2}$, and raised smoothly to a saturated value until the loading amount is $4.179 \times 10^{-9}$ mol cm$^{-2}$. Fig. S15b (ESI†) shows the activation process of the $P_8W_{48}$/rGO modified electrode with $P_8W_{48}$ loading of $1.393 \times 10^{-10}$ mol cm$^{-2}$ upon cycling between + 0.665 V and - 0.4 V versus RHE. Strikingly, the fully activated $P_8W_{48}$/rGO electrode always shows excellent HER performance (overpotentials of 70, 100 and 140 mV are required to reach the HER current densities of 10, 20 and 50 mA cm$^{-2}$ respectively) even at a very low loading amount of $P_8W_{48}$.

Controlled potential electrolysis was used to collect the evolved gas which was then analysed by gas chromatography. A movie showing hydrogen evolution occurred rapidly and at a high rate over the $P_8W_{48}$/rGO electrocatalytic film (Movie S1, ESI†). The detailed data are included in Fig. S16 (ESI†) and summarized here. The experiments carried out at different overpotentials confirm that hydrogen is produced with quantitative faradaic yield. For modified electrode containing $4.179 \times 10^{-9}$ mol cm$^{-2}$ of $P_8W_{48}$, 30.5 C was passed after 3600 s at $\eta = 295$ mV and 0.17 mmol of hydrogen were detected by gas chromatography corresponding to a faradaic yield of ca. 100% and a turnover frequency (TOF) as high as 11 s$^{-1}$ (TOF is defined as the number of moles of hydrogen per mole of $P_8W_{48}$ per second). The reproducibility of the observations was investigated by performing several experiments at different overpotentials with the same electrode.

It is worth noting that the high HER activity of $P_8W_{48}$/rGO is greatly due to the novel method we used for its synthesis. In particular, the use of the 16-electron electroreduced form of $P_8W_{48}$ ($P_8W_{48}$ (16 e$^-$)) as GO reductant is crucial. Indeed, both our reported electrochemical and photochemical synthetic routes for GO reduction via the less reduced form of the POM ($P_8W_{48}$ (8e$^-$)) yielded $P_8W_{48}$/rGO hybrids which did not feature any electrocatalytic performance towards the HER as evidenced by their electrochemical characteristics described in our previous report.[6] The XPS analysis of the $P_8W_{48}$/rGO/Nafion film (see details for the film formation in the experimental section 2.6) after the HER reveals the presence of W, C and O, and also F and S (attributed to Nafion) (Fig. S17a, ESI†). It should be noted that the P was too weak to be observed (see inset of Fig. S17a, ESI†) due to the low content of $P_8W_{48}$ in the film. However, the W *4f* spectra exhibits four new peaks attributed to W$^{IV}$ *4f* and W$^V$ *4f* besides those expected for the W$^{VI}$ *4f* centers of $P_8W_{48}$ (Fig. S17b, ESI†).[23] It is likely that the superior electrocatalytic performance of $P_8W_{48}$/rGO is, at least partly, due to the presence of tungsten in the low valence states V and IV. Work is in progress to get more inside into the electrocatalytic mechanistic pathway for the HER.

## 4. Conclusions

This work introduces the $P_8W_{48}$/rGO nanoassembly as an earth-abundant HER electrocatalyst with extremely high activity and very good stability. The HRTEM imaging and the solid state $^{31}$P NMR spectrum of $P_8W_{48}$/rGO reveal a strong interaction between individual $P_8W_{48}$ and transparent rGO sheets. The DFT calculations of the interaction between the building unit ($P_2W_{12}$) of $P_8W_{48}$ and G show that this interaction is strong. We provide experimental evidence for the predicted beneficial "microenvironment effect" for the HER resulting from the combination, in a 3D configuration, of high-quality rGO nanosheets and the well-dispersed $P_8W_{48}$ with good proton and electron reservoir abilities. Both of these properties of $P_8W_{48}$ are extraordinarily enhanced by the "microenvironment effect", which increase its basicity. Moreover, the excellent performance of the electrocatalyst is also attributed to further enhancement of its activity due to the presence of the rGO nanosheets, which maintain a high electrical conductivity of the overall electrode. Gas chromatography analysis coupled with bulk electrolysis confirmed the sustained production of hydrogen with quantitative faradaic yield and very high turnover

frequency at relatively low overpotential, in agreement with the Tafel parameters of $P_8W_{48}$/rGO. Altogether these observations suggest that the $P_8W_{48}$/rGO hybrid is potentially an attractive alternative to precious metal-based HER electrocatalysts, because $P_8W_{48}$ and $P_8W_{48}$/rGO can be synthesized in large scale via eco-friendly and simple methods.

## Acknowledgements

## References

1    J. D. Holladay, J. Hu, D. L. King and Y. Wang, *Catal. Today*, 2009, **139**, 244.

2    (a) A. J. Smith, Y. Chang, K. Raidongia, T. Chen, L. Li and J. Huang, *Adv. Energy Mater.*, 2014, **4**, DOI: 10.1002/aenm.201400398; (b) D. Kong, H. Wang, J. J. Cha, M. Pasta, K. J. Koski, J. Yao and Y. Cui, *Nano Lett.*, 2013, **13**, 1341; (c) Z. Chen, D. Cummins, B. N. Reinecke, E. Clark, M. K. Sunkara and T. F. Jaramillo, *Nano Lett.*, 2011, **11**, 4168; (d) Y. Li, H. Wang, L. Xie, Y. Liang, G. Hong and H. Dai, *J. Am. Chem. Soc.*, 2011, **133**, 7296; (e) J. Kibsgaard, Z. Chen, B. N. Reinecke and T. F. Jaramillo, *Nat. Mater.*, 2012, **11**, 963; (f) M. A. Lukowski, A. S. Daniel, F. Meng, A. Forticaux, L. Li and S. Jin, *J. Am. Chem. Soc.*, 2013, **135**, 10274; (g) Y. Yan, B. Xia, Z. Xu and X. Wang, *ACS Catal.*, 2014, **4**, 1693; (h) J. Kibsgaard and T. F. Jaramillo, *Angew. Chem. Int. Ed.*, 2014, **53**, 14433; (i) H. Wang, D. Kong, P. Johanes, J. J. Cha, G. Zheng, K. Yan, N. Liu and Y. Cui, *Nano Lett.*, 2013, **13**, 3426; (j) J. Kibsgaard, T. F. Jaramillo and F. Besenbacher, *Nat. Chem.*, 2014, **6**, 248; (k) M. Chhowalla, H. S. Shin, G. Eda, L. L. Li, K. P. Loh and H. Zhang, *Nat. Chem.*, 2013, **5**, 263; (l) D. Voiry, H. Yamaguchi, J. Li, R. Silva, D. C. B. Alves, T. Fujita, M. Chen, T. Asefa, V. B. Shenoy, G. Eda and M. Chhowalla, *Nat. Mater.*, 2013, **12**, 850.

3    (a) M. T. Pope, *Heteropoly and Isopoly Oxometalates*, Springer-Verlag, 1983; (b) B. Keita and L. Nadjo, In *Encyclopedia of Electrochemistry, Vol. 7* (Eds.: A. J. Bard, M. Stratmann), Wiley-VCH, Weinheim, 2006, p 607; (c) N. V. Izarova, M. T. Pope and U. Kortz, *Angew. Chem. Int. Ed.*, 2012, **51**, 9492; (d) A. Banerjee, B. S. Bassil, G. Röschenthaler and U. Kortz, *Chem. Soc. Rev.*, 2012, **41**, 7590; (e) H. N. Miras, J. Yan, D. Long and L. Cronin, *Chem. Soc. Rev.*, 2012, **41**, 7403; (f) A. Dolbecq, P. Mialane, F. Sécheresse, B. Keita and L. Nadjo, *Chem. Commun.*, 2012, **48**, 8299; (g) J. Lemonnier, S. Duval, S. Floquet and E. Cadot, *Isr. J. Chem.*, 2011, **51**, 290; (h) H. D. Pratt, N. S. Hudak, X. K. Fang and T. M. Anderson, *J. Power Source*, 2013, **236**, 259; (i) A. Sartorel, M. Bonchio, S. Campagna and F. Scandola, *Chem. Soc. Rev.*, 2013, **42**, 2262; (j) H. Lu, Y. V. Geletii, C. Zhao, J. W. Vickers, G. Zhu, Z. Luo, J. Song, T. Lian, D. G. Musaev and C. L. Hill, *Chem. Soc. Rev.*, 2012, **41**, 7572; (k) J. J. Stracke and R. G. Finke, *ACS Catal.*, 2014, **4**, 909; (l) Y. Yang, L. Yue, H. L. Li, E. Maher, Y. G. Li, Y. Z. Wang, L. X. Wu and V. W. W. Yam, *Small*, 2012, **8**, 3105; (m) J. C. Goloboy and W. G. Klemperer, *Angew. Chem. Int. Ed.*, 2009, **48**, 3562; (n) Polyoxometalates, Cluster Issue, (Guest Editors: U. Kortz and T. Liu), *Eur. J. Inorg. Chem.*, 2013, 1556-1967; (o) B. Keita, Y. W. Lu, L. Nadjo and R. Contant, *Electrochem. Commun.*, 2000, **2**, 720; (p) M. Jiang, D. Zhu, J. Cai, H. Zhang and X. Zhao, *J. Phys. Chem. C*, 2014, **118**, 14371.

4    (a) B. Keita, U. Kortz, L. R. Brudna Holzle, S. Brown and L. Nadjo, *Langmuir*, 2007, **23**, 9531; (b) M. Barsukova-Stuckart, N. V. Izarova, G. B. Jameson, V. Ramachandran, Z. Wang, J. van Tol, N. S. Dalal, R. Ngo Biboum, B. Keita, L. Nadjo and U. Kortz, *Angew. Chem. Int. Ed.*, 2011, **50**, 2639; (c) B. Nohra, H. El Moll, L. M. Rodriguez Albelo, P. Mialane, J. Marrot, C. Mellot-Draznieks, M. O'Keeffe, R. Ngo Biboum, J. Lemaire, B. Keita, L. Nadjo and A. Dolbecq, *J. Am. Chem. Soc.*, 2011, **133**, 13363; (d) W. Xu, C. Liu, W. Xing and T. Lu, *Electrochem. Commun.*, 2007, **9**, 180; (e) M. D. Symes and L. Cronin, *Nat. Chem.*, 2013, **5**, 403; (f) B. Rausch, M. D. Symes, G. Chisholm and L. Cronin, *Science*, 2014, **345**, 1326; ; (g) J-S. Qin, D-Y. Du, W. Guan, X-J. Bo, Y-F. Li, L-P. Guo, Z-M. Su, Y-Y. Wang, Y. Q. Lan and H-C. Zhou, *J. Am. Chem. Soc.*, 2015, **137**, 7169.

5    (a) W. J. Albery and A. R. Hillman, *Annu. Rep. Prog. Chem., Sect. C: Phys. Chem.*, 1981, **78**, 377; (b) F. C. Anson, J. M. Savéant and K. Shigehara, *J. Am. Chem. Soc.*, 1983, **105**, 1096; (c) F. C. Anson, J. M. Savéant and T. Ohsaka, *J. Am. Chem. Soc.*, 1983, **105**, 4883.

6    S. Li, R. Liu, R. N. Biboum, B. Lepoittevin, G. Zhang, A. Dolbecq, P. Mialane and B. Keita, *Eur. J. Inorg. Chem.*, 2013, 1882.

Energy & Environmental Science Accepted Manuscript

7    (a) C. N. R. Rao, A. K. Sood, K. S. Subrahmanyam and A. Govindaraj, *Angew. Chem. Int. Ed.,* 2009, **48**, 7752; (b) M. J. Allen, V. C. Tung and R. B. Kaner, *Chem. Rev.*, 2010, **110**, 132; (c) M. Pumera, *Chem. Soc. Rev.*, 2010, **39**, 4146; (d) X. Huang, X. Qi, F. Boey and H. Zhang, *Chem. Soc. Rev.*, 2012*,* **41**, 666; (e) Q. Xiang, J. Yu and M. Jaroniec, *Chem. Soc. Rev.*, 2012, **41**, 782; (f) H. Bai, C. Li and G. Shi, *Adv. Mater.*, 2011*,* **23**, 1089.

8    R. Contant and A. Tézé, *Inorg. Chem.*,1985, **24**, 4610.

9    B. Keita and L. Nadjo, *Mater. Chem. Phys.*, 1989, **22**, 77.

10   W. S. Hummers and R. E. Offeman, *J. Am. Chem. Soc.*, 1958, **80**, 1339.

11   H. Li, S. Pang, X. Feng, K. Müllen and C. Bubeck, *Chem. Commun.*, 2010, **46**, 6243.

12   D. Li, M. B. Müller, S. Gilje, R. B. Kaner and G. G. Wallace, *Nat. Nanotechnol.*, 2008, **3**, 101.

13   (a) S. Wang, H. Li, S. Li, F. Liu, D. Wu, X. Feng and L. Wu, *Chem. Eur. J.*, 2013, **19**, 10895; (b) R. Liu, S. Li, X. Yu, G. Zhang, S. Zhang, J. Yao, B. Keita, L. Nadjo and L. Zhi, *Small*, 2012, **8**, 1398.

14   S. Wen, W. Guan, J. Wang, Z. Lang, L. Yan and Z. Su, *Dalton Trans.*, 2012, **41**, 4602.

15   (a) P. Ordejón, E. Artacho and J. Soler, *Phys. Rev. B: Condens. Matter Mater. Phys*., 1996, **53**, R10441; (b) D. Sánchez-Portal, P. Ordejón, E. Artacho and J. M. Soler, *Int. J. Quantum Chem.,* 1997, **65**, 453; (c) J. M. Soler, E. Artacho, J. D. Gale, A. García, J. Junquera, P. Ordejón and D. Sánchez-Portal, *J. Phys.: Condens. Matter*, 2002, **14**, 2745.

16   J. P. Perdew, K. Burke and M. Ernzerhof, *Phys. Rev. Lett*., 1996, **77**, 3865.

17   (a) V. S. Korenev, S. Floquet, J. Marrot, M. Haouas, I. Mbomekallé, F. Taulelle, M. N. Sokolov, V. P. Fedin and E. Cadot, *Inorg. Chem.*, 2012, **51**, 2349; (b) U. Kortz and M. T. Pope, *Inorg. Chem.,* 1994, **33**, 5643.

18   T. Boyd, S. G. Mitchell, D. Gabb, D. Long and L. Cronin, *Chem. Eur. J.*, 2011, **17**, 12010.

19   J. Wang, S. Yang, D. Guo, P. Yu, D. Li, J. Ye and L. Mao, *Electrochem. Commun.*, 2009, **11**, 1892.

20   A. Mahmoud, B. Keita, L. Nadjo, O. Oung, R. Contant, S. Brown and  Y. de Kouchkovsky, *J. Electroanal.. Chem.,* 1999, **463**, 129.

21   M. A. Lukowski, A. S. Daniel, C. R. English, F. Meng, A. Forticaux, R. J. Hamers and S. Jin, *Energy Environ. Sci.*, 2014, **7**, 2608.

22   E. J. Popczun, C. G. Read, C. W. Roske, N. S. Lewis and R. E. Schaak, *Angew. Chem. Int. Ed.*, 2014, **53**, 5427.

23   (a) A. Katrib, F. Hemming, P. Wehrer, L. Hilaire and G. Maire, *J. Electron Spectrosc.*, 1995, **76**, 195; (b) S. C. Roy, R. Glaum, D. Abdullin, O. Schiemann, N. Q. Bac and K. Lii, *Z. Anorg. Allg. Chem.,* 2014, **640**, 1876; (c) P. Pérez-Romo, C. Potvin, J. Manoli and G. Djéga-Mariadassou, *J. Catal.*, 2002, **205**, 191; (d) Y. Hou, Y. Zhu, Y. Xu and X. Wang, *Appl. Catal. B: Environ.*, 2014, **156-157**, 122.